AGU PUBLICATIONS

Geophysical Research Letters

RESEARCH LETTER
10.1002/2016GL067978

Key Points:
- Rain-on-snow (ROS) events are identified in Sierra Nevada watersheds
- Atmospheric rivers (ARs) dramatically increase ROS occurrences
- ARs with and without ROS exhibit distinct differences over land and off shore

Correspondence to:
B. Guan,
bin.guan@jpl.nasa.gov

Citation:
Guan, B., D. E. Waliser, F. M. Ralph, E. J. Fetzer, and P. J. Neiman (2016), Hydrometeorological characteristics of rain-on-snow events associated with atmospheric rivers, *Geophys. Res. Lett.*, *43*, 2964–2973, doi:10.1002/2016GL067978.

Received 26 JAN 2016
Accepted 12 FEB 2016
Accepted article online 15 FEB 2016
Published online 29 MAR 2016

Hydrometeorological characteristics of rain-on-snow events associated with atmospheric rivers

Bin Guan[1,2], Duane E. Waliser[2,1], F. Martin Ralph[3], Eric J. Fetzer[2], and Paul J. Neiman[4]

[1]Joint Institute for Regional Earth System Science and Engineering, University of California, Los Angeles, California, USA, [2]Jet Propulsion Laboratory, California Institute of Technology, Pasadena, California, USA, [3]Center for Western Weather and Water Extremes, Scripps Institution of Oceanography, University of California, San Diego, La Jolla, California, USA, [4]Physical Sciences Division, Earth System Research Laboratory, NOAA, Boulder, Colorado, USA

Abstract Atmospheric rivers (ARs) are narrow, elongated, synoptic corridors of enhanced water vapor transport that play an important role in regional weather/hydrology. Rain-on-snow (ROS) events during ARs present enhanced flood risks due to the combined effects of rainfall and snowmelt. Focusing on California's Sierra Nevada, the study identifies ROS occurrences and their connection with ARs during the 1998–2014 winters. AR conditions, which occur during 17% of all precipitation events, are associated with 50% of ROS events (25 of 50). Composite analysis shows that compared to ARs without ROS, ARs with ROS are on average warmer by ~2 K, with snow water equivalent loss of ~0.7 cm/d (providing 20% of the combined water available for runoff) and ~50% larger streamflow/precipitation ratios. Atmospheric Infrared Sounder retrievals reveal distinct offshore characteristics of the two types of ARs. The results highlight the potential value of observing these events for snow, rain, and flood prediction.

1. Introduction

Atmospheric rivers (ARs) are narrow, elongated, synoptic corridors of enhanced water vapor transport that play an important role in regional weather and hydrology. Enhanced precipitation may occur when the moisture-laden ARs make landfall and interact with coastal and inland topography [*Ralph et al*., 2013; *Neiman et al*., 2013]. ARs deliver beneficial rain and snow to the semiarid western U.S. that form a crucial source of fresh water [*Guan et al*., 2010; *Dettinger et al*., 2011; *Rutz and Steenburgh*, 2012]. On the other hand, extreme precipitation associated with ARs can often lead to floods and related damages. *Ralph et al*. [2006] showed that all seven floods during water years (WY) 1998–2006 in the Russian River Basin in Northern California were associated with heavy rainfall produced by ARs. Similarly, *Neiman et al*. [2011] showed that 46 of 48 peak streamflow events during WY1998–2009 in western Washington were associated with ARs.

Compared to other winter storms, AR storms are typically warmer with a higher altitude of the melting level [e.g., *Neiman et al*., 2008, 2011; *Kim et al*., 2013; *Warner et al*., 2012]. Anomalously high melting levels associated with some ARs result in rain (instead of snow) falling at high elevations, thus leading to runoff over a much larger catchment area than during a typical storm. For example, the fractional catchment area contributing to runoff increases from 25% to 100%, as the melting level rises from 800 to 2800 m in the North Fork of the American River, California [*Lundquist et al*., 2008]. Increased runoff area in turn contributes to larger runoff volume. For example, river forecast model simulations showed that in three California watersheds the runoff volume tripled when the melting level rose by 600 m [*White et al*., 2002]. A flood-producing rain-on-snow (ROS) AR event in the Bernese Alps, Switzerland, was associated with a 1700 m rise in the melting level altitude within 24 h [*Rössler et al*., 2014].

Besides larger catchment areas contributing to runoff as a result of higher melting levels, rain falling on existing snow can lead to enhanced runoff due to melting of snow. The flood-producing ROS AR event in the Bernese Alps, Switzerland, mentioned above reduced snow depth by 40–60 cm at three meteorological stations within 6 h [*Rössler et al*., 2014]. A particularly warm ROS storm (which meets the AR criteria to be described later) in the Pacific Northwest melted 35–100% of the snowpack on the western slope of the northern and central Cascades and contributed to a flood event comparable in magnitude to the record in the Pacific Northwest [*Marks et al*., 1998].

It should be noted that the melting of snow by the transfer of heat from a liquid drop to frozen snow can be severely limited when the temperature of the drop is only a couple of degrees above freezing. In contrast, the

relatively warm ambient air and the condensation of vapor directly onto the snow surface can release large amounts of sensible and latent heat for the melting of snow [*Moore and Owens*, 1984, Table 1]. Such heat transfer between the air and the snow surface is plausibly substantial given the dew point temperature being above freezing and strong ventilation associated with the relatively windy conditions during ARs.

The form of AR precipitation (snow versus rain) and its impact on snowpack (accumulation versus melting) have important implications to water resource and flood management. Of particular interest here are ROS events during ARs, which present enhanced flood risks due to the combined effects of rainfall and snowmelt. ROS events during ARs have been documented largely in case studies [e.g., *Marks et al*., 1998; *Rössler et al*., 2014], and the climatological relationship between ROS and ARs remains to be understood, which motivates the current work. The objectives of this study are twofold: (1) to identify the climatological relationship between AR and ROS events in the Sierra Nevada and (2) to examine overland and offshore differences between ARs with ROS and ARs without ROS. The analysis period is WY1998–2014, for which a satellite-based record of landfalling ARs and observations of key variables of interest are available for the study area (see section 2).

2. Data and Methods

2.1. SNOTEL Stations

Measurements of daily snow water equivalent (SWE) and precipitation from 38 SNOw TELemetry (SNOTEL) [*Trabant and Clagett*, 1990] stations in the Sierra Nevada are obtained from the California Data Exchange Center (http://cdec.water.ca.gov). Each station consists of a snow pillow (Figure 1a, locations in green) and a colocated precipitation gauge (Figure 1a, black on green). All these stations are located above 1500 m elevation. Surface air temperature (SAT) readings are available at most of these stations (Figure 1a, red). Precipitation measurements from stations not tied to the SNOTEL sites (Figure 1a, black without green) are used together with the SNOTEL observations to calculate watershed mean precipitation. Nearly half of the precipitation measurements are from stations below 1500 m elevation. SWE and precipitation data during WY1998–2014 are used to match the period of the satellite AR landfall record (described below). SAT data are only available since WY2006. The SWE, precipitation, and SAT data were quality controlled following the procedures in *Serreze et al*. [1999], with 0.9/0.3/0.5% data discarded for the three variables, respectively.

2.2. Streamflow Gauges

Daily full natural flow values during WY1998–2014 are obtained from the California Data Exchange Center for 11 gauges (Figure 1a, purple). The gauges are located at major rivers along the western slope of the Sierra Nevada in 11 watersheds and operated by various government and private agencies. Full natural flow is computed by increasing/decreasing the gauged flow at each measurement point to account for upstream diversions, storage, and exchange of water with other watersheds, providing an estimate of the natural flow at the gauging locations had the flow not been altered by upstream human activities [*California Department of Water Resources*, 1982]. The full natural flow (hereafter, streamflow) data were quality controlled similar to the SNOTEL observations, with 3.6% data discarded. The streamflow values in volume per unit time were converted to depth (of runoff) per unit time by normalizing the values with the basin area above the elevation (i.e., upstream) of the streamflow gauge.

Streamflow/precipitation ratios are calculated from the normalized streamflow and mean precipitation averaged over all available stations within a given watershed. It is noted that the limited number of precipitation gauges in each watershed cannot possibly capture the large spatial variability of precipitation in these watersheds, and the gauges represent only a first-order estimate of the precipitation distributions. For a given day, the streamflow/precipitation ratio is calculated using the 2 day mean streamflow and precipitation averaged over that day and the following day, to accommodate some of the delayed responses in streamflow. Similar time windowing was used in *Neiman et al*. [2011] to associate the dates of AR landfalls with annual peak daily flows.

2.3. Atmospheric Temperature, Water Vapor, and Water Vapor Transport

The Atmospheric Infrared Sounder (AIRS) version-6 level-3 ($1° \times 1°$) standard retrievals [*Chahine et al*., 2006] provide temperature and water vapor at 12 pressure levels between 1000 and 100 hPa (unequally spaced by 50–150 hPa between each two levels), integrated water vapor (IWV), and SAT. Daily means are formed from weighted averages of the twice-daily satellite passes based on the number of data counts, to match

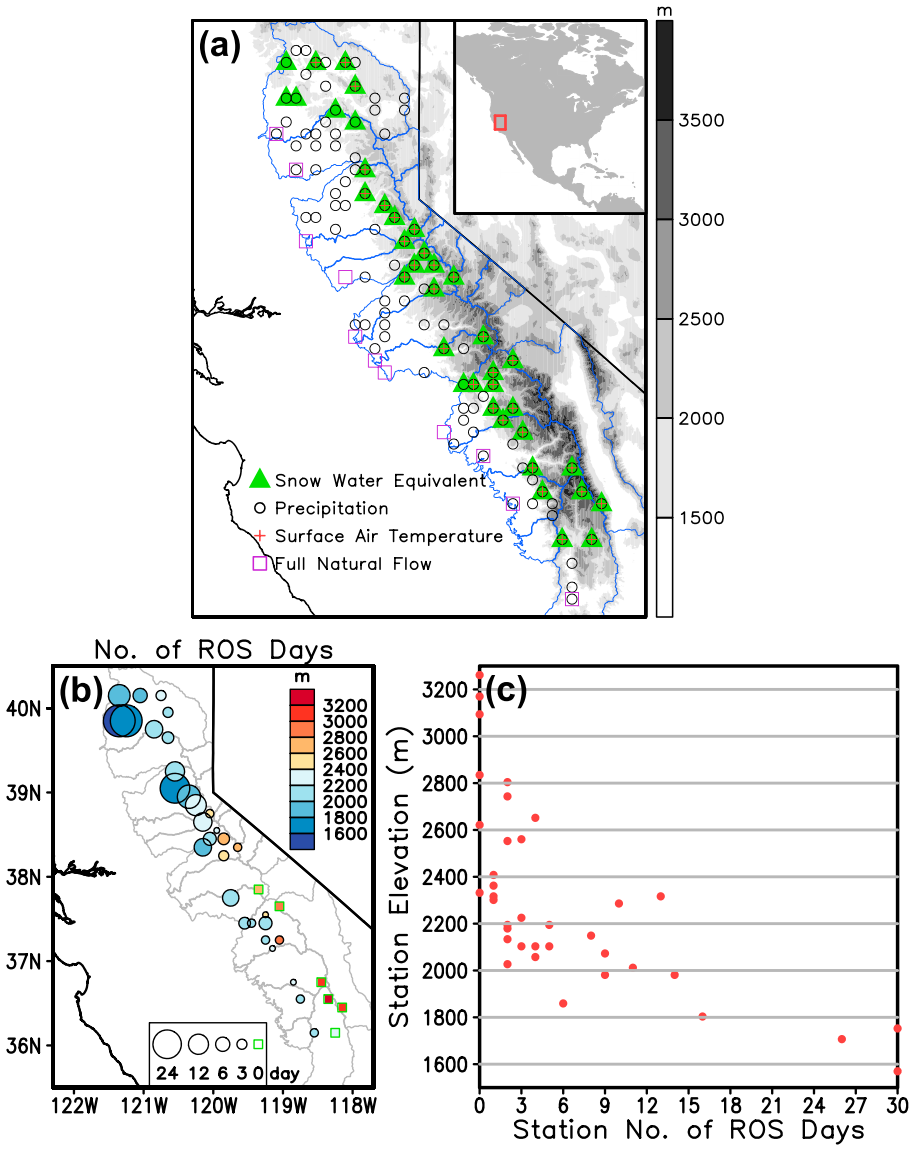

Figure 1. (a) Elevation (shading; m) map showing the Sierra Nevada area (20 watersheds delineated by the blue lines) and observation stations for SWE (green triangles), precipitation (black circles), SAT (red plus signs), and full natural flow (purple squares). (b) Number of ROS dates identified at each observation station during the winter months (November–March) of WY1998–2014. Black circles are sized proportional to the number of ROS dates, and green squares indicate the six stations where no ROS dates are identified during the period. Circles/squares are color filled according to the station elevation. (c) Number of ROS dates at each observation station as a function of the station elevation.

the temporal resolution of the other data used. The data are available since WY2003. Daily integrated water vapor transport (IVT) is derived from wind and specific humidity at 17 pressure levels between 1000 and 300 hPa provided by the ECMWF Re-Analysis Interim (ERA-Interim) [*Dee et al.*, 2011].

2.4. AR Landfall Record

Ralph et al. [2004] defined ARs as water vapor filaments longer than 2000 km in length, narrower than 1000 km in width, and with greater than 2 cm IWV. This definition was later used by *Neiman et al.* [2008] to create the satellite-based record of landfalling ARs onto the West Coast of North America. This record lists dates when a 2 cm IWV "river" intersects the coastline between 32.5 and 41°N (California landfalls) and between 41 and 52.5°N (Pacific Northwest landfalls) as observed by the Special Sensor Microwave Imager and the Special Sensor Microwave Imager/Sounder [*Kunkee et al.*, 2008]. This record now covers the period of WY1998–2014. Only California landfall dates are used in this study.

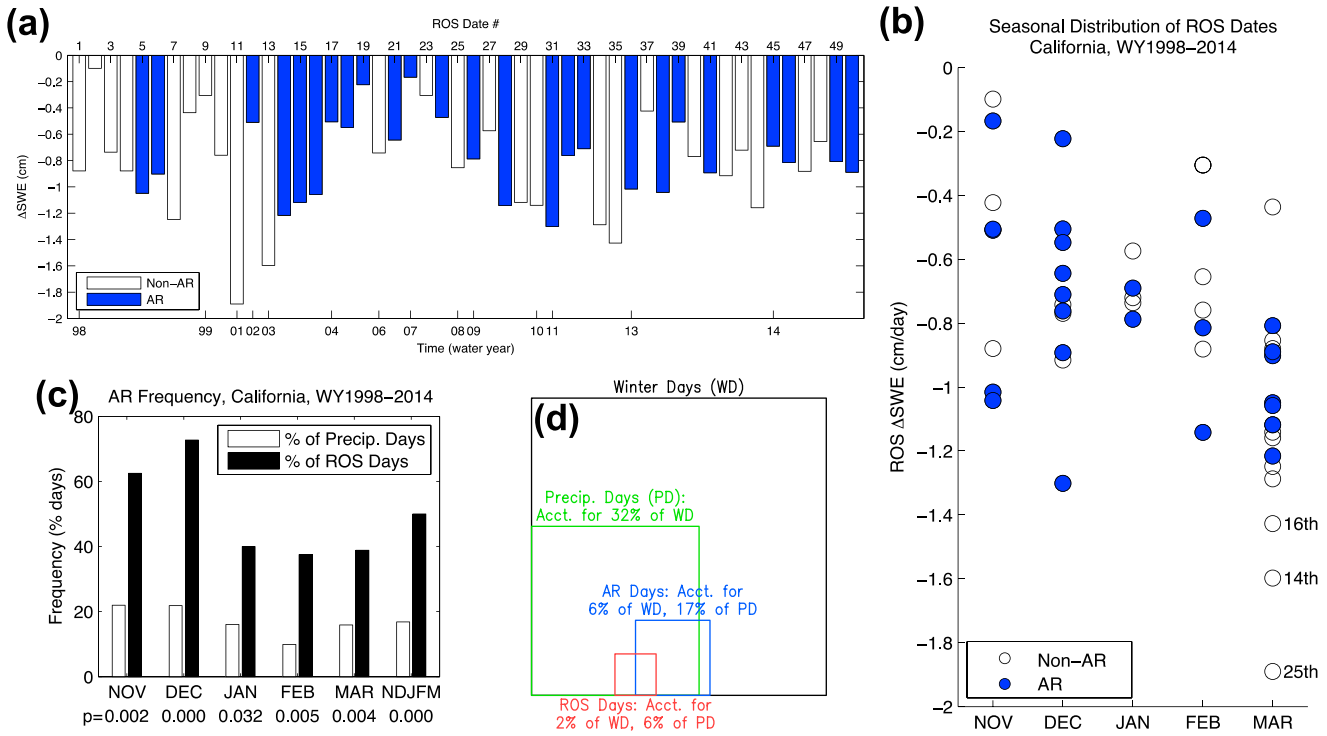

Figure 2. (a) ΔSWE (cm) during each of the 50 ROS dates identified. Numbers on the lower axis label give the first event in that water year. (b) Monthly distribution of ROS dates and associated ΔSWE (cm) values. The three ROS dates with the largest magnitude of ΔSWE are each labeled with the corresponding calendar day. AR (blue) and non-AR (white) dates are indicated in Figures 2a and 2b. (c) AR frequency (percent of days) as a function of month and type of precipitation conditions: precipitation days (white; a measure of the overall climatology), and ROS days (black); see text for definitions. *P* values calculated from the binomial cumulative distribution function indicate the probability that the fraction of AR dates from a random sample of precipitation days in a given month (with the sample size the same as in Figure 2b) could exceed the observed AR fraction in ROS days based on the general AR probability of occurrence in precipitation days of the given month. (d) The number of precipitation, AR, and ROS days relative to the total number of winter days. The area of each box is proportional to the associated number of days. The boxes are placed in a way consistent with the overlapping relationships between the various dates.

2.5. Definition of ROS Dates

ROS dates are defined using precipitation and SWE observations from the SNOTEL stations during the winter months of November to March, which is the primary snow season in the Sierra Nevada. Precipitation measurements are based on gauges with antifreeze that record the accumulated precipitation throughout the year [*Serreze et al.*, 1999]; direct detection and measurement of rainfall is not made at these stations. For a given station, ROS condition is defined if a notable amount of precipitation, i.e., >1 cm, falls during the day, while SWE is simultaneously reduced by any amount. ROS dates are then defined as the dates when the ROS condition is present at three or more stations within any 200 km zonal band. A similar approach was used in *McCabe et al.* [2007] in their definition of ROS based on the concurrence of precipitation and reduction in snow depth. As noted in *McCabe et al.* [2007], it is possible that some ROS events may not result in the reduction of SWE. However, our focus is on ROS events that do result in the melting of snow, which the above definition captures. A general precipitation date is defined using the same criteria except without the requirement for SWE loss. Non-ROS dates are defined as when no station shows ROS condition. Dates with ROS conditions present at only one or two stations are excluded from the analysis. The 1 cm/d threshold for precipitation is used in *Cohen et al.* [2015] in their definition of ROS and roughly equivalent to the 0.04 cm/h threshold used in *Lundquist et al.* [2008] to signify actual occurrence of precipitation based on gauge measurements in the Sierra Nevada; smaller precipitation values are deemed less reliable due to the overall difficulty in accurately measuring precipitation in snow-covered areas.

3. Overland Characteristics

ROS conditions have occurred at many stations in the Sierra Nevada in nearly all the watersheds with available SWE and precipitation data (Figure 1b). A larger number of events occur in the northern half of

the domain, where the elevation is generally lower. The two stations with the largest number of ROS occurrences (30 days during 17 years) are both located in the northernmost watershed and are among the few stations with elevation below 1800 m (Figures 1b and 1c). In general, stations at higher elevation have fewer ROS occurrences. ROS did not occur in the four stations above 2800 m during the analysis period. Almost all stations below 2800 m had at least one ROS date, with only two exceptions.

A total of 50 ROS dates is defined for WY1998–2014, with large year-to-year variability in the number of events (Figure 2a). The largest number of events occurred in WY1998 (eight dates) and WY2013 (nine dates), while no ROS events occurred in WY2000, WY2005, and WY2012. Reduction in SWE ranges between 0.1 and 1.9 cm/d, with notable event-to-event variability. Out of the 50 ROS dates, 25 (i.e., 50%) are also AR dates. Temperature information is not used in our ROS definition due to the shorter data record. It is nonetheless noted that during WY2006–2014 for which temperature measurements do exist, daily maximum temperatures at the SNOTEL stations were above freezing in all the ROS dates identified (not shown).

ROS occurs throughout the winter season (Figure 2b). March has the most monthly ROS occurrence, i.e., 18 dates in 17 years, which is about 2 to 4 times as frequently as in any of the first 4 months of the winter season. Seven out of the 18 ROS dates in March are AR dates. December has the second largest monthly ROS occurrence, with 8 out of the 11 ROS dates associated with ARs. Note that December is the month when ARs are climatologically the most frequent [*Guan et al*., 2013]. The monthly maximum (mean) daily reduction in SWE is 0.8–1.3 cm/d (0.6–0.7) during November–February and near 2 cm/d (1) in March. The three ROS dates with the largest reduction in SWE all occurred on non-AR dates in middle/late March in three different years, i.e., near the end of the snow season. In any month, the proportion of AR dates out of the ROS dates is significantly higher than would the proportion in a random sample of precipitation days (Figure 2c), suggesting a strong connection between ROS and ARs.

The relationship between ROS and ARs is further illustrated in Figure 2d, which shows the number of precipitation, AR, and ROS days relative to the total number of winter days. A small fraction of AR days fall outside of the defined precipitation days (i.e., a small fraction of the blue box falls outside of the green box); precipitation during those ARs was weak and did not meet the three station, 1 cm/d requirements (see section 2.5). As already shown in Figure 2a, AR frequency of occurrence is 50% in ROS days (percent of the red box overlapped by the blue box), which is ~3 times the general AR frequency of occurrence in precipitation days (17%; percent of the green box overlapped by the blue box). Conversely, ROS frequency is 15% in AR days (percent of the blue box overlapped by the red box), which is 2.5 times the general ROS frequency of occurrence in precipitation days (6%; percent of the green box overlapped by the red box). Given the strong correspondence between ROS and ARs, the subsequent analysis focuses on ARs with ROS versus ARs without ROS. The two types of events are of interest given the typical impact of ARs on both precipitation and runoff and the added flood risks when ROS happens.

Composite characteristics of SAT, ΔSWE, and streamflow/precipitation ratios are shown in Figure 3 for ARs with and without ROS. For ARs with ROS, only those stations meeting the ROS conditions (a minimum of three stations on any given ROS date) are included in the composite calculations. For ARs without ROS, the composite is displayed only for the stations appearing in the ROS composite to facilitate comparisons. Composite SAT during ARs with ROS is consistently above freezing across the domain, with an average of ~2.4°C (Figure 3a). Composite SAT during ARs without ROS is colder, with an average of ~0.2°C and mixed signs among different stations (Figure 3b). The temperature characteristics are broadly consistent with observations made at Donner Summit, California, by the *U.S. Army Corps of Engineers* [1956], which indicate that the probability of precipitation falling as rain or snow-rain mixture is less than 5% with SAT at 0°C, while at 2°C the probability is increased to 70% [*Lundquist et al*., 2008, Figure 10c]. Mean reduction in SWE is ~0.7 cm/d for ARs with ROS, about one half the mean SWE accumulation rate over ARs without ROS (Figures 3c and 3d). Composite precipitation at the ROS stations is 2.8 cm/d for ARs with ROS (not shown). In this regard, SWE loss contributes 20% of the combined water available for runoff (2.8 + 0.7 cm/d) at the ROS stations. Most of these stations are in wind-sheltered locations [*Farnes*, 1967], where snowmelt during precipitation events could be suppressed due to reduced wind speed and associated turbulent heat fluxes. The percent contribution of snowmelt to the combined water available for runoff can be much larger in unsheltered areas as observed during the 6 day ROS AR event in February 1996 [*Marks et al*., 1998]. Streamflow/precipitation ratios are on average ~50% larger during ARs with ROS than ARs without ROS (Figures 3e and 3f), an indication of additional streamflow contributed by rainfall and snowmelt in the snow zone.

) SAT (°C), (c and d) [illegible]E (cm/d),
3e) with ROS and (Figures 3b, 3d
ndicate stations where th[illegible]
e 95% level. Mark sizes are propo
rent between the rows. In each p
2014 for SAT and WY1998–2014 fo

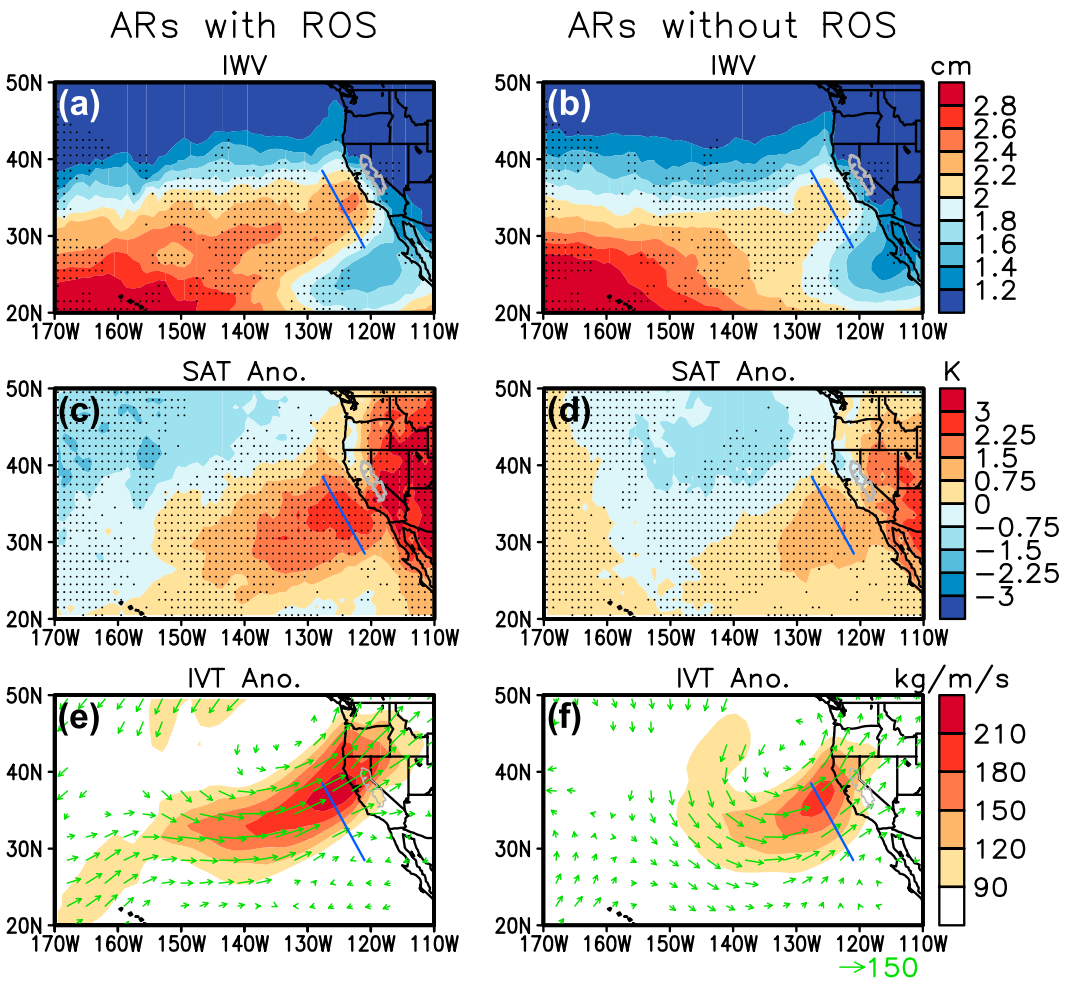

Figure 4. (a and b) Mean AIRS-derived IWV (cm) composited over ARs (Figure 4a) with ROS and (Figure 4b) without ROS. Stippling shows locations where the difference between (Figures 4a and 4b) is statistically significant at the 95% level. The Sierra Nevada area (Figure 1a, blue lines) is outlined in gray. The blue line indicates the location of the cross section used in Figure 5. (c and d) Same as Figures 4a and 4b but for composite AIRS SAT anomalies (K). (e and f) Composite ERA-Interim IVT anomalies (kg m^{-1} s^{-1}) over ARs (Figure 4e) with ROS and (Figure 4f) without ROS. Shading shows IVT magnitudes, and arrows show IVT magnitudes/directions. Arrows are shown only where the difference between Figures 4e and 4f is statistically significant at the 95% level for at least one component of IVT. Composite period is WY2003–2014 based on coverage of AIRS data. SAT and IVT anomalies are relative to the daily climatology.

It is noted that the distinction in streamflow/precipitation ratios between the two types of events is not pronounced in the southern watersheds, where the magnitudes of the ratios themselves are also small compared to the northern watersheds. This is consistent with the higher elevation at the more southern watersheds (Figure 1a, shading). Larger fractions of the basin area receive precipitation in the form of snow in these more southern, higher watersheds, leading to smaller streamflow/precipitation ratios. Also, less basin area experiences ROS in these higher watersheds, which contributes to smaller differences in streamflow/precipitation ratios between ROS and non-ROS events.

4. Offshore Characteristics

Composite plan-view analysis of IWV derived from AIRS exhibits the typical elongated structure associated with ARs in both ROS and non-ROS cases (Figures 4a and 4b). While the overall IWV patterns are similar, ARs with ROS carry more water vapor, with IWV larger by ~0.2 cm along the core section of AR composite. This is consistent with the close correlation between melting level altitude and IWV in ARs observed in the Bodega Bay-Cazadero area of California [*Neiman et al.*, 2009, Figure 9c]. Both types of composites are associated with warm SAT

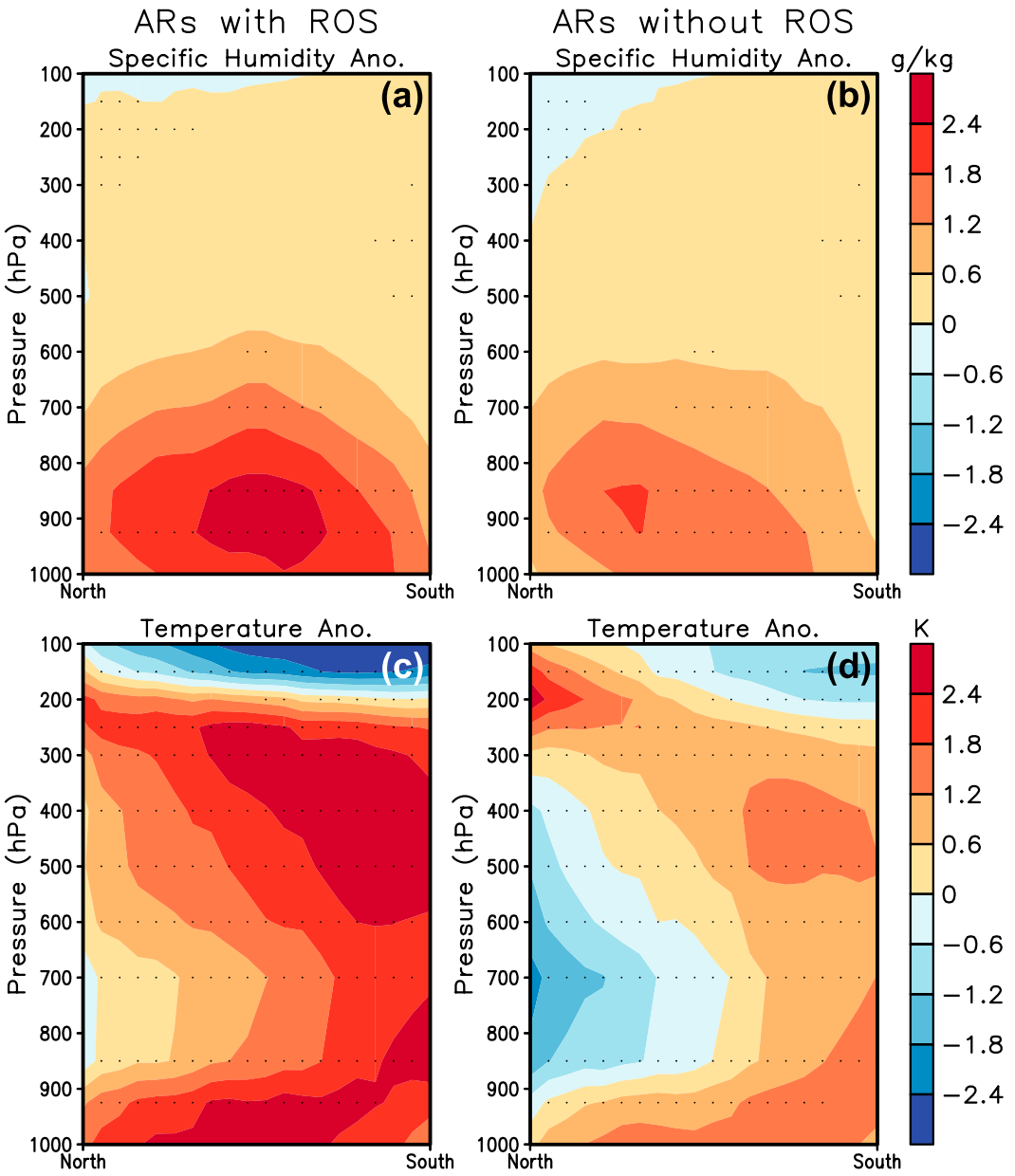

Figure 5. (a and b) Vertical cross section of mean anomalies of specific humidity (g/kg) along the blue line in Figure 4 composited over ARs (Figure 5a) with ROS and (Figure 5b) without ROS. Stippling shows locations where the difference between Figures 5a and 5b are statistically significant at the 95% level. (c and d) Same as Figures 5a and 5b but for composite temperature anomalies (K). Composite period is WY2003–2014 based on coverage of AIRS data. Anomalies are relative to the daily climatology.

anomalies (relative to the daily climatology) along the AR and extended overland (Figures 4c and 4d). Composite SAT anomalies are warmer by ~1.5 K in ARs with ROS, consistent with larger IWV in these cases. The differences in IWV and SAT anomalies are consistent with the composite IVT anomaly patterns, which show IVT anomalies directed from the tropics/subtropics (extratropics) in ARs with (without) ROS (Figures 4e and 4f).

Vertical cross sections of specific humidity and temperature anomalies (relative to the daily climatology) associated with ROS versus non-ROS ARs are shown in Figure 5. The cross sections are in the cross AR direction ~500 km off California where the contrast in SAT anomalies between the two types of events is the largest (Figure 4, blue lines). Near the center of positive anomalies at 900 hPa ARs with ROS are moister by ~1 g/kg compared to ARs without ROS (Figures 5a and 5b). Temperature anomaly patterns are characteristic of the

AR frontal structure, with warm anomalies at the surface, southward intrusion of cold anomalies around 700 hPa, and warm anomalies aloft (Figures 5c and 5d). Throughout the column, temperature anomalies are warmer by 1–2 K in the case of ROS ARs.

5. Conclusions

Focusing on California's Sierra Nevada where ARs have important impacts on the regional weather and hydrology, the current study identified ROS occurrences during the WY1998–2014 winters using observations of precipitation and SWE at 38 SNOTEL stations and established the connection between ROS and AR events using a satellite-based record of landfalling ARs along the California coast. ROS occurrence is dramatically increased from the general frequency of 6% in precipitation days to 15% during ARs. Out of the 50 ROS dates identified, 25 (i.e., 50%) are associated with AR landfalls, which is ~3 times the general AR frequency of occurrence during precipitation days (17%). ROS occurs most frequently in March (18 dates in 17 years), which is about 2 to 4 times as frequently as in any of the first 4 months of the winter season that we define as starting in November. In any month, the proportion of ARs in ROS days is significantly higher than the general AR frequency in precipitation days.

Composite analysis shows that ARs with ROS are warmer by ~2 K than ARs without ROS. SWE loss is ~0.7 cm/d during ARs with ROS, providing 20% of the combined water available for runoff (3.5 cm/d) at the observation stations (where snowmelt tends to be suppressed compared to unsheltered areas). Streamflow/precipitation ratio is ~50% larger during ARs with ROS versus ARs without ROS based on streamflow and precipitation data from 11 watersheds, indicating the combined contribution by rainfall (larger contributing area associated with higher melting level) and snowmelt to runoff. The AIRS satellite retrievals show distinct offshore characteristics of water vapor and temperature associated with the two types of ARs. The results highlight the potential value of observing these events for snow, rain, and flood prediction.

Acknowledgments
This research was supported by the NASA Energy and Water cycle Study (NEWS) program and the California Department of Water Resources. D.E. W.'s and E.J.F.'s contributions to this study were carried out on behalf of the Jet Propulsion Laboratory, California Institute of Technology, and F.M.R.'s at Scripps Institution of Oceanography, under a contract with the National Aeronautics and Space Administration.

References

California Department of Water Resources (1982), Unimpaired runoff data for the Sacramento, Feather, Yuba, and American rivers: 1906–1982, Rep. Resour. Agency, Sacramento, Calif.

Chahine, M. T., et al. (2006), AIRS: Improving weather forecasting and providing new data on greenhouse gases, *Bull. Am. Meteorol. Soc.*, *87*, 911–926, doi:10.1175/BAMS-87-7-911.

Cohen, J., H. Ye, and J. Jones (2015), Trends and variability in rain-on-snow events, *Geophys. Res. Lett.*, *42*, 7115–7122, doi:10.1002/2015GL065320.

Dee, D. P., et al. (2011), The ERA-Interim Reanalysis: Configuration and performance of the data assimilation system, *Q. J. R. Meteorol. Soc.*, *137*, 553–597, doi:10.1002/qj.828.

Dettinger, M. D., F. M. Ralph, T. Das, P. J. Neiman, and D. R. Cayan (2011), Atmospheric rivers, floods, and the water resources of California, *Water*, *3*, 445–478, doi:10.3390/w3020445.

Farnes, P. E. (1967), Criteria for determining mountain snow pillow sites Proc. 35th Western Snow Conf., Boise, ID, Western Snow Conference, 59–62.

Guan, B., N. P. Molotch, D. E. Waliser, E. J. Fetzer, and P. J. Neiman (2010), Extreme snowfall events linked to atmospheric rivers and surface air temperature via satellite measurements, *Geophys. Res. Lett*, *37*, L20401, doi:10.1029/2010GL044696.

Guan, B., N. P. Molotch, D. E. Waliser, E. J. Fetzer, and P. J. Neiman (2013), The 2010/2011 snow season in California's Sierra Nevada: Role of atmospheric rivers and modes of large-scale variability, *Water Resour. Res.*, *49*, 6731–6743, doi:10.1002/wrcr.20537.

Kim, J., D. E. Waliser, P. J. Neiman, B. Guan, J.-M. Ryoo, and G. A. Wick (2013), Effects of atmospheric river landfalls on the cold season precipitation in California, *Clim. Dyn.*, *40*, 465–474, doi:10.1007/s00382-012-1322-3.

Kunkee, D. B., G. A. Poe, D. J. Boucher, S. D. Swadley, Y. Hong, J. E. Wessel, and E. A. Uliana (2008), Design and evaluation of the first Special Sensor Microwave Imager/Sounder, *IEEE Trans. Geosci. Remote Sens.*, *46*, 863–883, doi:10.1109/TGRS.2008.917980.

Lundquist, J. D., P. J. Neiman, B. Martner, A. B. White, D. J. Gottas, and F. M. Ralph (2008), Rain versus snow in the Sierra Nevada, California: Comparing Doppler profiling radar and surface observations of melting level, *J. Hydrometeorol.*, *9*, 194–211, doi:10.1175/2007JHM853.1.

Marks, D., J. Kimball, D. Tingey, and T. Link (1998), The sensitivity of snowmelt processes to climate conditions and forest cover during rain-on-snow: A case study of the 1996 Pacific Northwest flood, *Hydrol. Processes*, *12*, 1569–1587, doi:10.1002/(SICI)1099-1085(199808/09)12:10/11<1569::AID-HYP682>3.0.CO;2-L.

McCabe, G. J., L. E. Hay, and M. P. Clark (2007), Rain-on-snow events in the western United States, *Bull. Am. Meteorol. Soc.*, *88*, 319–328, doi:10.1175/BAMS-88-3-319.

Moore, R. D., and I. F. Owens (1984), Controls on advective snowmelt in a maritime alpine basin, *J. Climate Appl. Meteorol.*, *23*, 135–142, doi:10.1175/1520-0450(1984)023<0135:COASIA>2.0.CO;2.

Neiman, P. J., F. M. Ralph, G. A. Wick, J. D. Lundquist, and M. D. Dettinger (2008), Meteorological characteristics and overland precipitation impacts of atmospheric rivers affecting the West Coast of North America based on eight years of SSM/I satellite observations, *J. Hydrometeorol.*, *9*, 22–47, doi:10.1175/2007JHM855.1.

Neiman, P. J., A. B. White, F. M. Ralph, D. J. Gottas, and S. I. Gutman (2009), A water vapor flux tool for precipitation forecasting, *Water Manage.*, *162*, 83–94, doi:10.1680/wama.2009.162.2.83.

Neiman, P. J., L. J. Schick, F. M. Ralph, M. Hughes, and G. A. Wick (2011), Flooding in western Washington: The connection to atmospheric rivers, *J. Hydrometeorol.*, *12*, 1337–1358, doi:10.1175/2011JHM1358.1.

Neiman, P. J., M. Hughes, B. J. Moore, F. M. Ralph, and E. M. Sukovich (2013), Sierra barrier jets, atmospheric rivers and precipitation characteristics in Northern California: A composite perspective based on a network of wind profilers, *Mon. Weather Rev.*, *141*, 4211–4233, doi:10.1175/MWR-D-13-00112.1.

Ralph, F. M., P. J. Neiman, and G. A. Wick (2004), Satellite and CALJET aircraft observations of atmospheric rivers over the eastern North Pacific Ocean during the winter of 1997/98, *Mon. Weather Rev.*, *132*, 1721–1745, doi:10.1175/1520-0493(2004)132<1721:SACAOO>2.0.CO;2.

Ralph, F. M., P. J. Neiman, G. A. Wick, S. I. Gutman, M. D. Dettinger, D. R. Cayan, and A. B. White (2006), Flooding on California's Russian River: Role of atmospheric rivers, *Geophys. Res. Lett.*, *33*, L13801, doi:10.1029/2006GL026689.

Ralph, F. M., T. Coleman, P. J. Neiman, R. Zamora, and M. D. Dettinger (2013), Observed impacts of duration and seasonality of atmospheric-river landfalls on soil moisture and runoff in coastal Northern California, *J. Hydrometeorol.*, *14*, 443–459, doi:10.1175/JHM-D-12-076.1.

Rössler, O., P. Froidevaux, U. Börst, R. Rickli, O. Martius, and R. Weingartner (2014), Retrospective analysis of a nonforecasted rain-on-snow flood in the Alps—A matter of model limitations or unpredictable nature?, *Hydrol. Earth Syst. Sci.*, *18*, 2265–2285, doi:10.5194/hess-18-2265-2014.

Rutz, J. J., and W. J. Steenburgh (2012), Quantifying the role of atmospheric rivers in the interior western United States, *Atmos. Sci. Lett.*, *13*, 257–261, doi:10.1002/asl.392.

Serreze, M. C., M. P. Clark, R. L. Armstrong, D. A. McGinnis, and R. S. Pulwarty (1999), Characteristics of the western United States snowpack from snowpack telemetry (SNOTEL) data, *Water Resour. Res.*, *35*, 2145–2160, doi:10.1029/1999WR900090.

Trabant, D. C., and G. P. Clagett (1990), Measurement and evaluation of snowpacks, in *Cold Regions Hydrology and Hydraulics*, edited by W. L. Ryan and R. D. Crissman, pp. 39–93, American Society of Civil Engineers, New York.

U.S. Army Corps of Engineers (1956), *Snow Hydrology: Summary Report of the Snow Investigations*, 437 pp., North Pacific Division, Corps of Engineers, U.S. Army, Portland, Oreg.

Warner, M. D., C. F. Mass, and E. P. Salathé (2012), Wintertime extreme precipitation events along the Pacific Northwest coast: Climatology and synoptic evolution, *Mon. Weather Rev.*, *140*, 2021–2043, doi:10.1175/MWR-D-11-00197.1.

White, A. B., D. J. Gottas, E. T. Strem, F. M. Ralph, and P. J. Neiman (2002), An automated brightband height detection algorithm for use with Doppler radar spectral moments, *J. Atmos. Oceanic Technol.*, *19*, 687–697, doi:10.1175/1520-0426(2002)019<0687:AABHDA>2.0.CO;2.